High-resolution supernova neutrino spectra represented by a simple fit

Irene Tamborra,[1] Bernhard Müller,[2] Lorenz Hüdepohl,[2] Hans-Thomas Janka,[2] and Georg Raffelt[1]

[1]*Max-Planck-Institut für Physik (Werner-Heisenberg-Institut), Föhringer Ring 6, 80805 München, Germany*
[2]*Max-Planck-Institut für Astrophysik, Karl-Schwarzschild-Str. 1, 85748 Garching, Germany*
(Dated: January 9, 2013)

To study the capabilities of supernova neutrino detectors, the instantaneous spectra are often represented by a quasi-thermal distribution of the form $f_\nu(E) \propto E^\alpha e^{-(\alpha+1)E/E_{\rm av}}$ where $E_{\rm av}$ is the average energy and α a numerical parameter. Based on a spherically symmetric supernova model with full Boltzmann neutrino transport we have, at a few representative post-bounce times, re-converged the models with vastly increased energy resolution to test the fit quality. For our examples, the spectra are well represented by such a fit in the sense that the counting rates for a broad range of target nuclei, sensitive to different parts of the spectrum, are reproduced very well. Therefore, the mean energy and root-mean-square energy of numerical spectra hold enough information to provide the correct α and to forecast the response of multi-channel supernova neutrino detection.

I. INTRODUCTION

The neutrino signal from the next nearby core-collapse supernova (SN) remains the most coveted target for low-energy neutrino astronomy. Galactic SNe are rare, perhaps a few per century, and such an observation will be a once-in-a-lifetime opportunity to look deeply inside a collapsing star and learn about its astrophysical workings as well as about neutrino properties. Several detectors worldwide are in operation that will register a high-statistics signal while others are in preparation or under discussion [1].

In order to assess the physics potential of various detectors or detection principles one needs the expected flavor-dependent SN neutrino flux spectra. In the absence of self-consistent three-dimensional core-collapse simulations there is no standard SN neutrino flux model and moreover, the flavor-dependent flux spectra depend on the properties of the incompletely known neutron-star equation of state, on the properties of the collapsing star, notably its mass, and, of course, on time for any given case. In this situation parametric studies, taking account of the plausible range of predictions, are the preferred course of action.

We here address one particular aspect of such studies, i.e. the plausible spectral shape of SN neutrino fluxes. On a rough level of approximation, the spectra follow a thermal distribution that can be described in terms of an effective temperature. In detail the spectra formation is a complicated process, different energy groups emerging from different depths in the proto-neutron star atmosphere [2, 3], and a more refined description is necessary for a more detailed understanding.

The next level of sophistication is to describe the non-equilibrium spectra by a three-parameter fit that allows for deviations from a strictly thermal spectrum [4]. One particularly simple realization are spectra where the energy-dependent neutrino number flux for each flavor has the form [3]

$$f_\nu(E) \propto E^\alpha \, e^{-(\alpha+1)E/E_{\rm av}} . \qquad (1)$$

Here, $E_{\rm av}$ is the average energy and α a numerical parameter describing the amount of spectral pinching; the value $\alpha = 2$ corresponds to a Maxwell-Boltzmann spectrum, and $\alpha = 2.30$ to a Fermi-Dirac distribution with zero chemical potential. In general the neutrino spectra are fitted by $2 \leq \alpha \leq 4$ [3] with higher $\alpha > 2$ indicating stronger pinching and $\alpha < 2$ meaning anti-pinching relative to a Maxwell-Boltzmann distribution. The three parameters $E_{\rm av}$, α, and the overall normalization can be determined, for example, if a numerical SN simulation provides the energy flux (luminosity) L_ν in some flavor, the average energy $E_{\rm av} = \langle E_\nu \rangle$ and some other energy moment, for example $\langle E_\nu^2 \rangle$ or sometimes $\langle E_\nu^3 \rangle$.

While spectra of the form of Eq. (1) certainly provide a reasonable overall representation, it is not obvious how well the spectral tails are reproduced. For studying detector responses with target nuclei with a significant energy threshold, it is imperative that the accuracy of the α-fit in the high-energy tail be checked against solutions of the neutrino transport equations. This is especially relevant for example for lead in the Halo detector [5], argon in future large-scale liquid argon detectors [6], or subdominant detection channels on oxygen in water Cherenkov detectors [7] or on carbon in liquid scintillator detectors [8].

Modern numerical SN codes treat neutrino transport with Boltzmann solvers that are expected to produce physically accurate spectra. On the other hand, neutrino transport is the most CPU-time consuming aspect of SN simulations so that in practice the energy resolution is limited. For example, in typical simulations of the Garching group, 17–21 energy bins are used, corresponding to an energy resolution $\Delta\epsilon/\epsilon \sim 0.3$. Whether such a (seemingly) coarse zoning is adequate for modeling the high-energy tail of the spectrum and hence for judging the quality of α-fits needs to be determined at least once

by a resolution study. Spectra from standard resolution (SR) neutrino transport simulations are therefore of little value for assessing the quality of α-fits in the spectral tail, as are Monte Carlo studies [3, 4], which suffer from limited sampling at high energies.

In this paper, we investigate whether α-fits and SR spectra from SN simulations are sufficiently accurate to predict detection rates that are sensitive to the high-energy tail. To this end, we study the spectral shape and its impact on the relative detector response of different materials using *high-resolution* (HR) spectra computed for a few representative post-bounce times of a representative spherically symmetric simulation. These spectra have been obtained by re-converging models at a given post-bounce time after refining the energy binning. With the HR spectra we can then test how well a global fit of the form of Eq. (1) reproduces the relative neutrino counting rates of different materials that probe rather different parts of the spectrum.

We always ignore the effect of neutrino flavor conversions. The ordinary Mikheyev-Smirnov-Wolfenstein (MSW) effect [9, 10] or self-induced flavor conversions [11] strongly modify the flavor-dependent spectra seen by a detector on Earth [12]. For example, the detectable $\bar{\nu}_e$ flux will be a certain linear combination of the $\bar{\nu}_e$ and $\bar{\nu}_x$ spectra emitted at the source. These detection spectra need not be represented by a simple fit, in particular if self-induced conversions cause features such as "spectral splits." Determining the detection spectra in terms of the source spectra is the task of oscillation studies, usually performed by post-processing the fluxes provided by numerical models. Justifying simple representations of the source spectra for the purpose of flavor conversion studies is one prime motivation for our work.

To this end we describe in Sec. II our numerical SN model and in Sec. III the target materials. A comparison between counting rates based on the numerical spectra and the fitted ones is performed in Sec. IV before concluding in Sec. V.

II. NUMERICAL SUPERNOVA MODEL

We have performed simulations of the $15 M_\odot$ progenitor of Woosley and Weaver [13] with the neutrino hydrodynamics code PROMETHEUS-VERTEX [14], which solves the 0th and 1st neutrino moment equations with a variable Eddington factor closure that is provided by the formal solution of a simplified (model) Boltzmann equation. The explosion of the spherically symmetric model was artificially initiated 500 ms after bounce. For the dynamical evolution of the model including the feedback into the hydrodynamics, we used 21 energy bins with a typical resolution $\delta\epsilon/\epsilon$ (ratio of zone width to zone mean energy) of ~ 0.29. We refer to this setup as the SR case.

In order to accurately predict the shape of the neutrino spectra, particularly in the high-energy tail, we computed high-resolution (HR) stationary solutions of the neutrino transport equations for a representative time during the accretion phase (261 ms after bounce) and for the proto-neutron star cooling phase (1016 ms and 1991 ms) using the matter background from the dynamical simulation. Different from the dynamical run, the original treatment of [14] for the Doppler and redshift terms is used instead of that of [15], and the threshold values for the monochromatic neutrino energy density below which a spectral extrapolation is performed has been reduced by a factor of 100. We also transition continuously from the comoving frame to the lab frame once neutrino interactions cease in order to eliminate artifacts due to the velocity jump in the shock. These numerical changes accelerate convergence and help to obtain smoother and more accurate spectra.

The spacing of the logarithmic energy grid was much finer with 42 bins and $\delta\epsilon/\epsilon = 0.11$ in the HR case. For better comparison, the stationary solutions for the SR case were re-computed with precisely the same numerics. Figure 1 shows the obtained HR spectra for the species ν_e, $\bar{\nu}_e$, and ν_x (with ν_x meaning a *single* kind of ν_μ, $\bar{\nu}_\mu$, ν_τ, and $\bar{\nu}_\tau$).

In order to compare the numerical spectra (histograms) with a quasi-thermal fit of the form of Eq. (1), we determine the parameter α in terms of the energy moments of the distribution. One way of fixing α is to use the energy moment of order k and notice that

$$\frac{\langle E_\nu^k \rangle}{\langle E_\nu^{k-1} \rangle} = \frac{k+\alpha}{1+\alpha} \langle E_\nu \rangle. \tag{2}$$

We have checked that for our cases the implied value of α does not strongly depend on k, which already implies that this type of fit is a reasonable representation. In the following we will use $k = 2$, i.e., the relation

$$\frac{\langle E_\nu^2 \rangle}{\langle E_\nu \rangle^2} = \frac{2+\alpha}{1+\alpha}. \tag{3}$$

We show examples of the fits as continuous colored curves alongside the HR spectra (step functions) on a logarithmic and on a linear scale in Figs. 1 and 2, respectively. For comparison we also show the SR spectra and their correspondent fits as thin dashed black lines in Fig. 1, and find that visually the fits work very well in both cases. Values for the fit parameter α, the luminosity L_ν, and the neutrino mean energy $\langle E_\nu \rangle$ for the three snapshots and for the different neutrino species ν_e, $\bar{\nu}_e$, and ν_x are listed in Table I both for the HR and the SR case. We note that despite the lower energy resolution, the SR spectra from the dynamical simulation typically give very similar luminosities and mean energies, which are consistent with the HR case within $\sim 5\%$ or less. The fit parameter α agrees similarly well except for ν_e in the post-explosion phase with a deviation of up to 9%. However, this is due to a very steep dependence of α on the second energy moment, $\langle E_\nu^2 \rangle$, when the energy ratio in Eq. (3) is close to unity, and does not affect the fit curves appreciably.
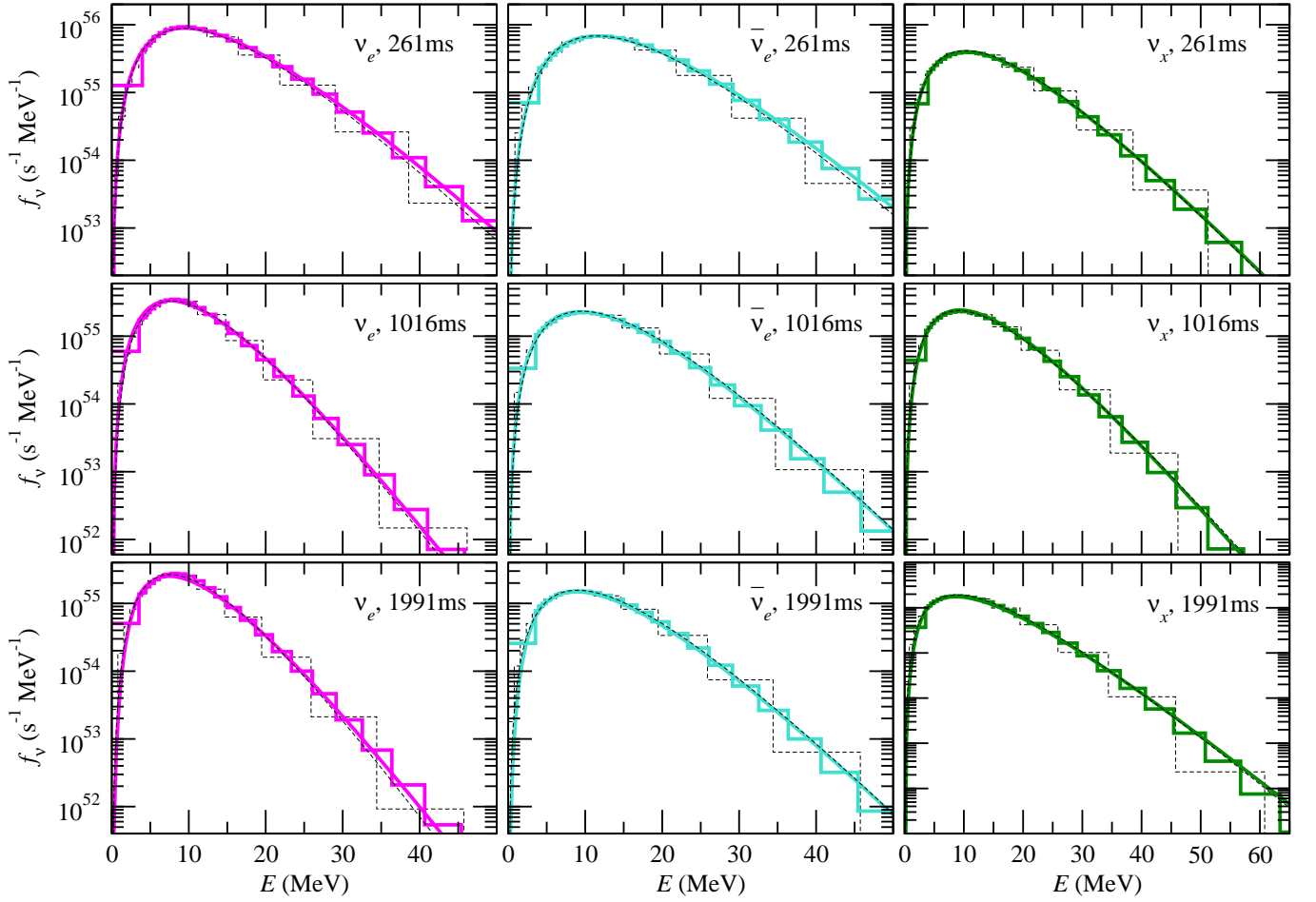
FIG. 1: Spectra for species ν_e (left column), $\bar{\nu}_e$ (middle column) and ν_x (right column) for post-bounce times of 261 (top row), 1016 (middle row), and 1991 ms (bottom row). The data from the PROMETHEUS-VERTEX spectra are shown as step functions, and the continuous curves are quasi-thermal fits according to Eq. (1). Thick magenta, turquoise, and green lines are used for the different neutrino species (ν_e, $\bar{\nu}_e$ and ν_x, respectively) in the HR case, while the SR spectra and fits are shown as thin dashed black lines.

TABLE I: Fit parameters α, luminosities L_ν, and neutrino mean energies $\langle E_\nu \rangle$ for different neutrino species and post-bounce times for HR and SR spectra.

t [ms]	species	α_{HR}	α_{SR}	$L_{\nu,\mathrm{HR}}$ [$10^{52}\,\mathrm{erg\,s^{-1}}$]	$L_{\nu,\mathrm{SR}}$ [$10^{52}\,\mathrm{erg\,s^{-1}}$]	$\langle E_\nu \rangle_{\mathrm{HR}}$ [MeV]	$\langle E_\nu \rangle_{\mathrm{SR}}$ [MeV]
261	ν_e	2.65	2.73	2.80	2.68	13.05	12.87
261	$\bar{\nu}_e$	3.13	3.23	2.79	2.71	15.23	15.05
261	ν_x	2.42	2.48	1.58	1.63	14.48	14.48
1016	ν_e	2.90	3.14	0.62	0.62	10.14	10.28
1016	$\bar{\nu}_e$	2.78	2.88	0.67	0.70	12.69	12.87
1016	ν_x	2.39	2.52	0.75	0.77	12.89	13.00
1991	ν_e	2.92	3.17	0.48	0.47	10.01	10.01
1991	$\bar{\nu}_e$	2.61	2.67	0.44	0.44	12.28	12.36
1991	ν_x	2.34	2.49	0.54	0.55	12.31	12.39

III.   DETECTION CROSS SECTIONS

In existing detectors, SN neutrinos are primarily measured in the $\bar{\nu}_e$ channel by virtue of the inverse beta decay (IBD) reaction $\bar{\nu}_e + p \rightarrow n + e^+$. The cross section varies roughly as E_ν^2 so that the overall event rate is well reproduced, if the SN neutrino spectrum is approximated
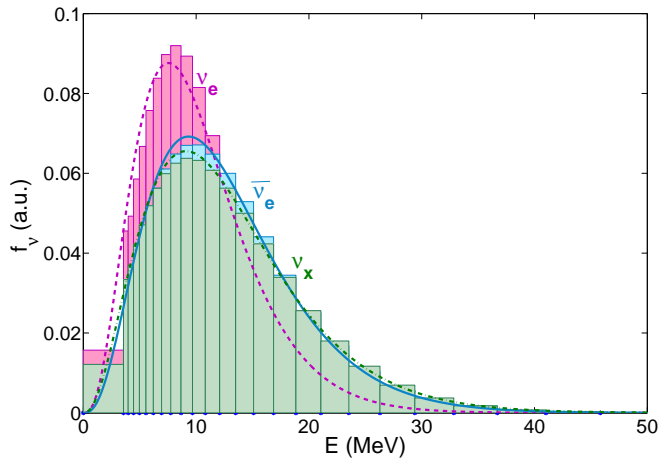
FIG. 2: Spectra for species ν_e, $\bar{\nu}_e$ and ν_x. Histograms are the PROMETHEUS-VERTEX HR spectra of our model at time 1016 ms. The curves are quasi-thermal fits according to Eq. (1): dashed for ν_e, continuous for $\bar{\nu}_e$, and dot-dashed for ν_x.
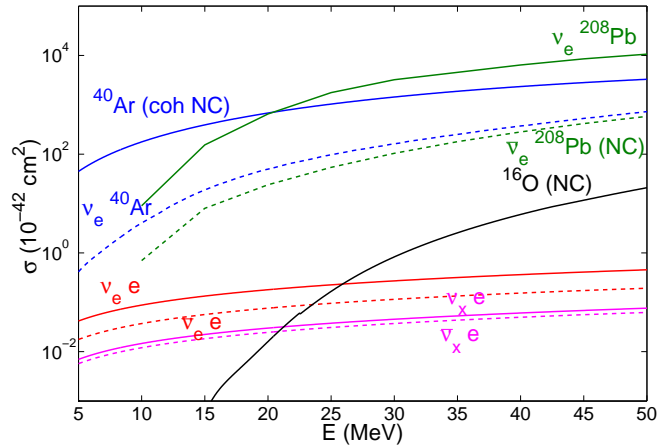

FIG. 3: Neutrino cross sections on some representative target nuclei (see text for details).

by a quasi-thermal spectrum where the second energy moment is used to determine α.

However, other detection channels are also of interest. One is elastic scattering on electrons where the cross section varies roughly linearly with E_ν. Of greater interest for our purpose of testing the goodness of the α-fit are reactions with a higher energy threshold or steeper energy variation than IBD. One example is the recently built HALO detector in SNOLAB where 79 tons of lead are used as target material. Other examples are reactions on argon in future liquid argon detectors that are primarily considered in the context of long-baseline neutrino oscillation studies and reactions on oxygen in water Cherenkov detectors and on carbon in liquid scintillator detectors.

In our study we consider several selected reactions that

span a broad range of spectral responses to neutrino fluxes and show the energy-dependent cross sections in Fig. 3. The reaction sensitive to the lowest range of energies is elastic scattering on electrons via both charged-current (CC) and neutral-current (NC) for ν_e and $\bar{\nu}_e$ and via NC interaction for ν_x [16].

In nuclei, CC interactions proceed via $\nu_e + (N, Z) \rightarrow (N-1, Z+1)+e^-$ and $\bar{\nu}_e+(N,Z) \rightarrow (N+1, Z-1)+e^+$, respectively. The $\bar{\nu}_e$ interaction is typically suppressed at a given energy with respect to the ν_e interaction due to Pauli blocking. Neutral current interactions may also produce observable signals via ejected nucleons or de-excitation photons. As one example we consider NC interactions with ^{16}O [7, 17–19], which is relevant for water-based detectors.

Interactions with heavier nuclei, such as lead, may yield quite high rates of both CC and NC interactions. Observable signatures include leptons and ejected nucleons. Single and multiple neutron ejections are possible. The relevant interactions for lead-based detectors are $\nu_e + {}^A\text{Pb} \rightarrow e^- + {}^A\text{Bi}^*$ and $\nu_x + {}^A\text{Pb} \rightarrow \nu_x + {}^A\text{Pb}^*$. For both CC and NC cases, the resulting nuclei de-excite via neutron emission. Antineutrino CC interactions are strongly suppressed. Although natural lead contains isotopes other than ^{208}Pb, the neutron cross section for $A = 208$ should be similar to other components. For the Pb cross sections see Refs. [20–23].

Liquid argon detectors will have excellent sensitivity to ν_e via the CC interaction $\nu_e + {}^{40}\text{Ar} \rightarrow e^- + {}^{40}\text{K}^*$. This is an interaction for which the de-excitation γs from ^{40}K* can be observed. The reaction $\bar{\nu}_e + {}^{40}\text{Ar} \rightarrow e^+ + {}^{40}\text{Cl}^*$ will also occur and can be tagged via the pattern of γs. NC excitations are possible, although little information is available in the literature because of the low-energy nuclear recoils that make it practically difficult to detect. Energy thresholds as low as few MeV may be possible. Although the chances for detecting such a reaction are rather low, we consider NC coherent scattering anyway as an example of a reaction scanning the low-energy region of the neutrino spectra. The cross sections are reported in Refs. [6, 24–27].

For the different channels that we consider, we use the cross sections as in [1]. They have been used in the SNOWGLOBES software package [28].

IV. COUNTING RATES

The detector counting rate as a function of incoming neutrino energy is proportional to $f_\nu(E)\sigma(E)$. Based on the numerical neutrino spectra for the 1016 ms model, we show this quantity in Fig. 4 for our suite of interaction processes, normalized to the maximum rate of each process. This plot demonstrates that the different detection processes probe vastly different parts of the neutrino spectra.

We now compare the total counting rates for each of our reactions using as a neutrino spectrum either the
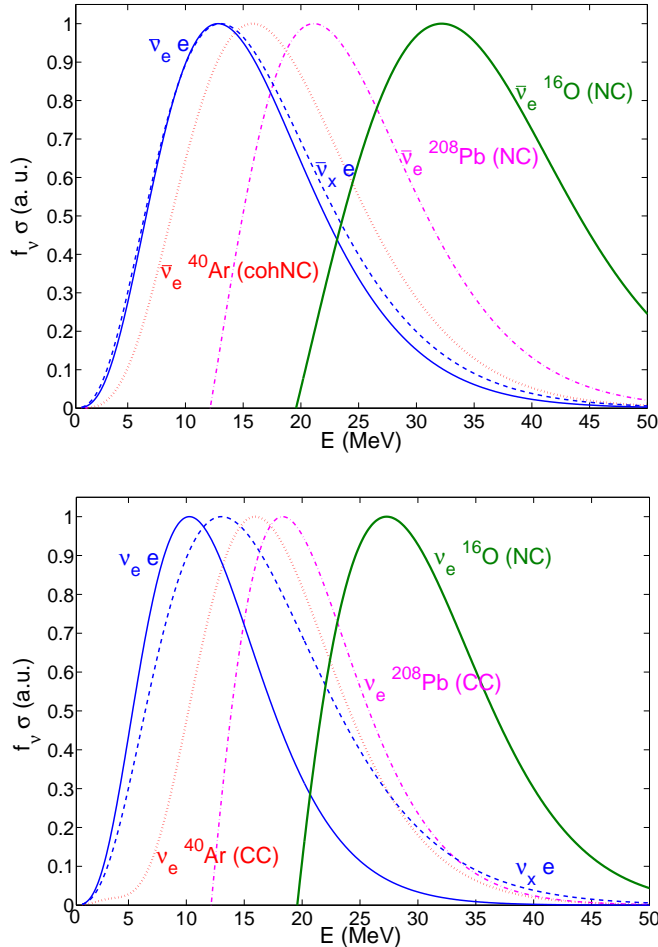
FIG. 4: Detection rate as a function of neutrino energy for different reactions, based on our 1016 ms model. Each curve is normalized to its maximum. *Top:* Anti-neutrinos. *Bottom:* Neutrinos.

moments of the numerical distribution, is sufficiently ac-

TABLE II: Ratio of counting rate based on our spectral fit and the direct numerical HR spectrum, $N_{\rm fit}/N_{\rm num}$.

t[ms]	$\nu_e{}^{40}$Ar CC	$\nu_e{}^{208}$Pb CC	$\nu_e e$	$\nu_x e$	$\nu_e{}^{16}$O NC
261	1.01	1.02	1.00	1.00	1.01
1016	1.02	1.06	1.01	1.00	0.91
1991	1.02	1.07	1.01	1.00	0.90
t[ms]	$\bar{\nu}_e{}^{40}$Ar NC	$\bar{\nu}_e{}^{208}$Pb NC	$\bar{\nu}_e e$	$\bar{\nu}_x e$	$\bar{\nu}_e{}^{16}$O NC
261	1.00	1.02	1.00	1.00	1.05
1016	1.01	1.03	1.00	1.00	1.16
1991	1.00	1.03	1.00	1.00	1.18

curate to predict the detector response for target nuclei with relatively high threshold energies. In order to answer this question reliably, we have produced high-resolution (HR) neutrino spectra at several postbounce times of a spherically symmetric SN simulation. In addition, these spectra have allowed us to check for the first time whether the coarser standard resolution (SR) of typical supernova models (which is dictated by strong CPU-time limitations) already allows robust signal predictions.

We have compared SR and HR spectra and fitted both with the analytic fit of Eq. (1), based on the first two energy moments of the numerical distribution. These fitted spectra account well for the detection rates in SN neutrino detectors with vastly different target nuclei. We conclude that for the purpose of signal forecast in different detectors reasonably good accuracy can be achieved by considering the lowest two energy moments of numerically produced spectra. Moreover, we have verified that a modest standard energy resolution as affordable in typical supernova simulations already gives energy moments surprisingly close to the HR case. This insight simplifies parametric studies of detection forecasts for the neutrino signal from the next nearby SN because it is sufficient to represent the non-equilibrium spectra by a simple three-parameter quasi-thermal fit.

numerical output directly (rate $N_{\rm num}$) compared with the rate inferred if the spectrum is represented by our fit function (rate $N_{\rm fit}$). In Table II, we report the ratio $N_{\rm fit}/N_{\rm num}$ for neutrinos (top part) and antineutrinos (bottom part). The agreement between $N_{\rm num}$ and $N_{\rm fit}$ is very good and typically the error is only a few percent. Even for the oxygen reaction, which probes the highest-energy tail of all examples, the difference is only some 10–20%. Assuming complete flavor conversions due to neutrino oscillations ($\nu_e \rightarrow \nu_x$, and the same for antineutrinos), we tested that the ratio $N_{\rm fit}/N_{\rm num}$ differs from the ones reported in Table II only on the level of tenths of a percent (results not shown here). Such a result further confirms the good quality of the alpha-fit.

V. CONCLUSIONS

In this paper, we have investigated whether the simple analytic fit of Eq. (1), based on the first two energy

[1] K. Scholberg, Annu. Rev. Nucl. Part. Sci. **62** (2012) 81. [arXiv:1205.6003].

[2] G. G. Raffelt, Astrophys. J. **561** (2001) 890.

[3] M. T. Keil, G. G. Raffelt and H.-T. Janka, Astrophys. J. **590** (2003) 971.

[4] H.-T. Janka and W. Hillebrandt, Astron. Astrophys. **224** (1989) 49.

[5] D. Väänänen and C. Volpe, JCAP **1110**, 019 (2011).

[6] I. Gil Botella and A. Rubbia, JCAP **0408** (2004) 001.

[7] K. Langanke, P. Vogel and E. Kolbe, Phys. Rev. Lett. **76** (1996) 2629.

[8] M. Wurm *et al.* [LENA Collaboration], Astropart. Phys. **35** (2012) 685.

[9] S. P. Mikheev and A. Yu. Smirnov, Yad. Fiz. **42**, (1985) 1441 [Sov. J. Nucl. Phys. **42** (1985) 913].

[10] L. Wolfenstein, Phys. Rev. D **17** (1978) 2369.

[11] H. Duan, G. M. Fuller and Y.-Z. Qian, Ann. Rev. Nucl. Part. Sci. **60** (2010) 569.

[12] G. Fogli, E. Lisi, A. Marrone and I. Tamborra, JCAP **0904** (2009) 030.

[13] S. E. Woosley and T. A. Weaver, Astrophys. J. Suppl. **101** (1995) 181.

[14] M. Rampp and H.-T. Janka, Astron. Astrophys. **396** (2002) 361.

[15] B. Müller, H. Dimmelmeier and H.-T. Janka, Astrophys. J. Suppl. **189** (2010) 104.

[16] W. J. Marciano and Z. Parsa, J. Phys. G **29** (2003) 2629.

[17] E. Kolbe, K. Langanke and P. Vogel, Phys. Rev. D **66** (2002) 013007.

[18] W. C. Haxton and C. Johnson, Phys. Rev. Lett. **65** (1990) 1325.

[19] W. C. Haxton, Phys. Rev. C **37** (1988) 2660.

[20] G. M. Fuller, W. C. Haxton and G. C. McLaughlin, Phys. Rev. D **59** (1999) 085005.

[21] E. Kolbe and K. Langanke, Phys. Rev. C **63** (2001) 025802.

[22] J. Toivanen, E. Kolbe, K. Langanke, G. Martinez-Pinedo and P. Vogel, Nucl. Phys. A **694** (2001) 395.

[23] A. R. Samana and C. A. Bertulani, Phys. Rev. C **78**, 024312 (2008).

[24] R. S. Raghavan, Phys. Rev. D **34** (1986) 2088.

[25] I. Gil Botella and A. Rubbia, JCAP **0310** (2003) 009.

[26] A. Bueno, I. Gil Botella and A. Rubbia, hep-ph/0307222.

[27] M. S. Athar and S. K. Singh, Phys. Lett. B **591** (2004) 69.

[28] http://www.phy.duke.edu/~schol/snowglobes.